European Conference on Computational Fluid Dynamics
ECCOMAS CFD 2006
P. Wesseling, E. Oñate and J. Périaux (Eds)

ON THE TREATMENT OF COMPLEX GEOMETRIES IN A CARTESIAN GRID FLOW SOLVER WITH THE LEVEL SET METHOD

Olivier Botella* **and Yoann Cheny**

LEMTA - UMR 7563 CNRS-INPL-UHP
2, avenue de la Forêt de Haye, B.P 160
54504 Vandœuvre-lès-Nancy, France
*e-mail: Olivier.Botella@ensem.inpl-nancy.fr

Key words: Cartesian grid, Complex geometry, Immersed boundary, Level set, Finite volumes, Incompressible viscous flow

Abstract. *We present a new Cartesian grid method for the computation of incompressible viscous flows in irregular geometries. The irregular boundary is implicitly represented by its signed distance function (the level-set function) and, by using level-set calculus tools, we are able to preserve the Cartesian structure of the discretized Navier-Stokes equations. The resulting linear systems are efficiently solved with a black box multigrid solver for structured grids. The method is validated for the circular cylinder flow at low Reynolds number.*

1 INTRODUCTION

Much attention has recently been devoted to the extension of Cartesian grid flow solvers to complex geometries by immersed boundary (IB) methods (see Mittal and Iaccarino[12] for a recent review). In these methods, the irregular boundary is not aligned with the computational grid, and the treatment of the cells which are cut by the boundary remains an important issue. Indeed, the discretization in these cut-cells should be designed such that : (a) the overall accuracy of the method is not severely diminished and (b) the high computational efficiency of the structured solver is preserved.

Two major classes of IB methods can be distinguished on the basis of their treatment of cut-cells. Classical IB methods use a finite volume/difference structured solver in Cartesian cells away from the irregular boundary, and discard the discretization of flow equations in the cut-cells[5]. Instead, special interpolations are used for setting the value of the dependent variables in the latter cells. Thus, strict conservation of quantities such as mass and momentum is not observed near the irregular boundary. Numerous revisions of these interpolations are still proposed for improving the accuracy and consistency of this class of IB methods[9]. A second class of IB methods (also called cut-cell methods[4,15]) aims for actually discretizing the flow equations in cut-cells. However, the calculation of fluxes in cut-cells relies usually on unstructured techniques, and their negative impact on the computational efficiency of the code is difficult to evaluate.

The purpose of this communication is to present a new IB method for incompressible viscous flows which takes the best aspect of both approaches. As the cut-cell method in Dröge and Verstappen[4], our method is based on the symmetry preserving finite-volume discretization on Cartesian grids by Verstappen and Veldman[17]. However, the major difference is that we have undertaken representing the irregular boundary by its level-set function[13]. With the help of level-set calculus tools, the fluxes in Cartesian and cut-cells are discretized in a unified fashion. The Cartesian structure of the discrete systems is thus preserved, and they are efficiently solved with black box solvers for structured grids. The method is validated for the circular cylinder flow at low Reynolds number, which has become the standard benchmark test for IB methods.

2 Numerical method

Let Ω be a rectangular computational domain and Γ its surface. The governing equations are the incompressible Navier-Stokes equations in integral form. In the following, we will consider the finite-volume discretization of the continuity equation :

$$\int_\Gamma \boldsymbol{v} \cdot \boldsymbol{n} \ \mathrm{d}S = 0, \tag{1}$$

where $\boldsymbol{v} = (u, v)$ is the velocity, and of the u-momentum equation :

$$\frac{\mathrm{d}}{\mathrm{d}t} \int_\Omega u \ \mathrm{d}V + F^{\mathrm{c}} + \int_\Gamma p \, \boldsymbol{e}_x \cdot \boldsymbol{n} \ \mathrm{d}S - \frac{1}{\mathrm{Re}} F^{\mathrm{d}} = 0, \tag{2}$$

where p is the pressure, Re is the Reynolds number, F^{c} and F^{d} are the convective and diffusive flux, respectively given by :

$$F^{\mathrm{c}} \equiv \int_\Gamma (\boldsymbol{v} \cdot \boldsymbol{n}) \, u \ \mathrm{d}S, \tag{3a}$$

$$F^{\mathrm{d}} \equiv \int_\Gamma \boldsymbol{\nabla} u \cdot \boldsymbol{n} \ \mathrm{d}S. \tag{3b}$$

Basic discretization on the MAC mesh

The Cartesian method on which our IB method is based is the second-order finite volume discretization of Verstappen and Veldman[17], which has the ability to preserve on non-uniform cell distributions the conservation properties (for total mass, momentum and kinetic energy) of the original MAC method[8]. The staggered arrangement of the discrete velocities on the MAC mesh is illustrated in Fig. 1. The computational domain

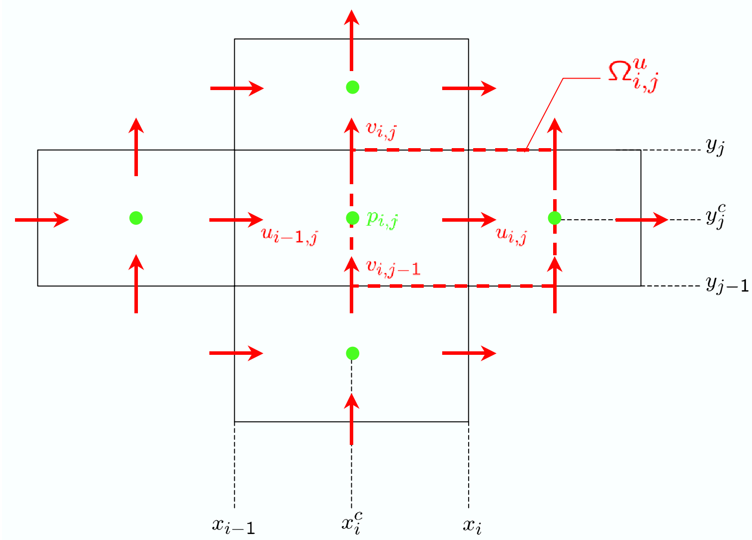

Figure 1: Location of the variables in cell $\Omega_{i,j}$ on the MAC mesh.

is divided in non-uniform Cartesian cells $\Omega_{i,j} = \left] x_{i-1}\,,\, x_i \right[\times \left] y_{j-1}\,,\, y_j \right[$, of size $\Delta x_i \Delta y_j$, and center $\boldsymbol{x}^{\mathrm{c}}_{ij} = (x^{\mathrm{c}}_i\,,\, y^{\mathrm{c}}_j)$. The surface of cell $\Omega_{i,j}$ is divided in 4 elementary faces as $\Gamma_{i,j} = \Gamma_{\mathrm{e}} \cup \Gamma_{\mathrm{w}} \cup \Gamma_{\mathrm{n}} \cup \Gamma_{\mathrm{s}}$ using the usual compass notations (see *e.g.* Ferziger and Perič[6], Chap. 3). Cell $\Omega_{i,j}$ is used as the control volume for discretizing the continuity equation (1), while the staggered control volume $\Omega^u_{i,j} = \left] x^{\mathrm{c}}_i\,,\, x^{\mathrm{c}}_{i+1} \right[\times \left] y_{j-1}\,,\, y_j \right[$, of size $\widetilde{\Delta x_i} \Delta y_j$, is used for the u-momentum equation (2). Compass notations will be used for intermediate steps of the discretization of (2). For example, we will denote $F^{\mathrm{d}}_{\mathrm{n}}$ the diffusive flux (3b) through the north face Γ^u_{n}, *i.e.* :

$$F^{\mathrm{d}}_{\mathrm{n}} \equiv \int_{x^{\mathrm{c}}_i}^{x^{\mathrm{c}}_{i+1}} \frac{\partial u}{\partial y}(x, y_j)\,\mathrm{d}x. \tag{4}$$

The LS-MAC mesh for discretization in irregular domains

We consider now an irregular fluid domain Ω^{f} which is embedded in the computational domain Ω. To keep track of the irregular boundary Γ^{f}, we employ a signed distance function ϕ (*i.e.* , the level set function[7,13]) such that ϕ is negative in the fluid region Ω^{f}, ϕ is positive in the solid region $\Omega^{\mathrm{s}} = \Omega \setminus \Omega^{\mathrm{f}}$, and such that the boundary Γ^{f} corresponds to the zero level-set of this function, *i.e.* :

$$\phi(\boldsymbol{x}) \equiv \begin{cases} -\Delta, & \boldsymbol{x} \in \Omega^{\mathrm{f}}, \\ 0, & \boldsymbol{x} \in \Gamma^{\mathrm{f}}, \\ +\Delta, & \boldsymbol{x} \in \Omega^{\mathrm{s}}, \end{cases} \tag{5}$$

where Δ is the distance from $\boldsymbol{x}$ to the closest point on the irregular boundary. This leads to the modification of the MAC mesh that is described in Fig. 2, and that will be subsequently referred to as the LS-MAC mesh. In this figure, the cell $\Omega_{i,j}$ which is part fluid/part solid, is commonly called a cut cell. The discretization of the fluxes in cut cells is performed with the help of an additional variable, denoted $\phi_{i,j}$, that stores the values of the level-set function ϕ at the upper right corner of the cells. The level-set values are used to efficiently compute quantities relevant to the irregular boundary, such as outward normal vectors or surface integrals over Γ^{f}, *etc...* But the most important quantity for

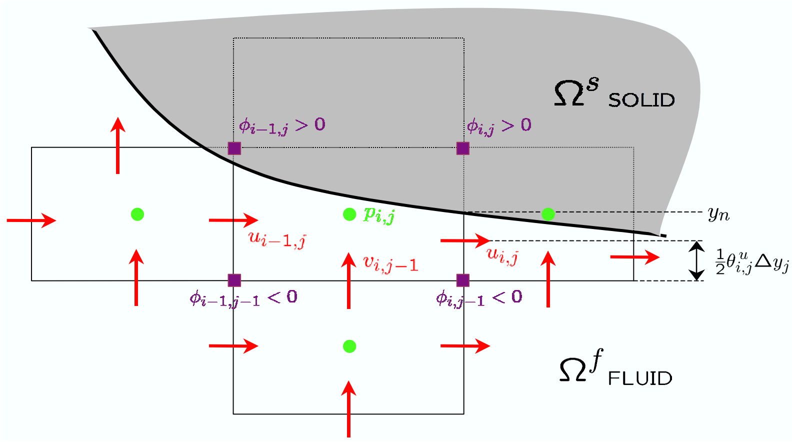

Figure 2: Location of the variables in the cut cell $\Omega_{i,j}$ on the LS-MAC Mesh. The intersection of the east face Γ_{e} with the irregular boundary is (x_i, y_{n}). See Fig. 1 for complementary notations.

the discretization of the fluxes is the fluid portion of the cell faces. For example in Fig. 2, by using one-dimensional linear interpolation of $\phi(x_i, y)$ in $[y_{j-1},\, y_j]$, the length of the face Γ_{e} which belongs to the fluid domain is :

$$y_n - y_{j-1} = \theta^u_{i,j}\ \Delta y_j, \qquad \text{with } \theta^u_{i,j} = \frac{\phi_{i,j-1}}{\phi_{i,j-1} - \phi_{i,j}},$$

since $\phi(x_i, y_n) = 0$. The quantity $\theta^u_{i,j} \in \big[0, 1\big]$ is called the cell-face ratio. It has been used by Gibou et al.[7] to impose boundary conditions for finite difference discretizations of the Poisson and heat equation in irregular domains. In the present work, it shall be used to :

- Detect whether the discrete velocities in the LS-MAC mesh are in the fluid region. For example in Fig. 2, velocity $u_{i,j}$ has to be computed since $\theta^u_{i,j} > 0$, but $v_{i,j}$ should not since $\theta^v_{i,j} = 0$.
- Discretize surface fluxes such as (3) near the irregular boundary, and implement boundary conditions.
- Compute global quantities of interest such as forces or moments acting on the irregular boundary, and auxiliary variables such as vorticity or stream-function.

- Interpolate all flow variables at cell corners for visualization purpose.

These last two points will be discussed in a forthcoming paper[3]. In the following, we shall use the cell-face ratios for discretizing the surface fluxes (1), (3a) and (3b) of the Navier-Stokes equations. It will be shown that the concept of cell face ratio generalizes Cartesian discretizations : when the cell faces are totally in the fluid region ($\theta = 1$) or aligned ($\theta = 0$) with the solid boundary, our method recovers the second-order discretization of Verstappen and Veldman[17] on the MAC mesh.

Discretization of the continuity equation

As in the Cartesian case, the starting point of the LS-MAC discretization concerns the continuity equation (1), that reads in cell $\Omega_{i,j}$:

$$\overline{u}_{i,j} - \overline{u}_{i-1,j} + \overline{v}_{i,j} - \overline{v}_{i,j-1} = 0, \tag{6}$$

where mass fluxes across cell faces are denoted with a bar ; for example the mass flux through the east face Γ^u_{e} in Fig. 2 is :

$$\overline{u}_{i,j} \equiv \int_{y_{j-1}}^{y_{\mathrm{n}}} u(x_i, y)\ \mathrm{d}y. \tag{7}$$

In order to easily discretize this integral, we first locate $u_{i,j}$ in the middle of the fluid part of the face :

$$u_{i,j} \equiv u(x_i, y_{j-1} + \tfrac{1}{2}\,\theta^u_{i,j}\,\Delta y_j), \tag{8}$$

then, by using midpoint quadrature, we finally get :

$$\overline{u}_{i,j} \cong \theta^u_{i,j}\,\Delta y_j u_{i,j}. \tag{9}$$

After similar calculations for the other cell faces, the discretization of (6) is :

$$\mathrm{Cont}(\Omega_{i,j}) \equiv \Delta y_j \big(\,\theta^u_{i,j}\,u_{i,j} - \,\theta^u_{i-1,j}\,u_{i-1,j}\big) + \Delta x_i \big(\,\theta^v_{i,j}\,v_{i,j} - \,\theta^v_{i,j-1}\,v_{i,j-1}\big) = 0. \tag{10}$$

As an exemple, if we consider the cut cell of Fig. 2, the discrete continuity equation reads there :

$$\Delta y_j \big(\,\theta^u_{i,j}\,u_{i,j} - \,\theta^u_{i-1,j}\,u_{i-1,j}\big) + \Delta x_i \big(0 - v_{i,j-1}\big) = 0,$$

and, in the case of a Cartesian cell ($\theta = 1$ or $\theta = 1$), the discrete continuity equation reduces to the standard MAC discretization.

Discretization of the diffusive fluxes

In the MAC method, the discretization of the fluxes in the u-momentum equation are performed in the control volume $\Omega^u_{i,j}$ that fits in the fluid domain, see Fig. 1. This discretization has to be extended to the cut cell of Fig. 2. However, trying to fit exactly the shape of $\Omega^u_{i,j}$ within the irregular fluid domain Ω^{f} would lead to a non-rectangular control volume, and the Cartesian data structure would thus be lost. Instead, we shall keep the control volume rectangular, and take care that our discretization in the cut cells preserves the symmetries of the Navier-Stokes system, as advocated by Verstappen and Veldman[17]. Thus, the discretization of the diffusive fluxes (3b) in $\Omega^u_{i,j}$ should read :

$$\int_{\Gamma^u} \boldsymbol{\nabla} u \cdot \boldsymbol{n} \; \mathrm{d}S \cong \mathcal{K}U, \tag{11}$$

where U is the vector that stores the discrete velocities and $\mathcal{K}$ is a sparse symmetric definite positive matrix, with five non-zero coefficients in 2D. We note that $\mathcal{K}$ is a symmetric matrix if, for all lines (i,j) of the system $\mathcal{K}U = \mathrm{RHS}$ written in compass notation as :

$$\mathcal{K}_{\mathrm{E}}(i,j)u_{i+1,j} + \mathcal{K}_{\mathrm{W}}(i,j)u_{i-1,j} + \mathcal{K}_{\mathrm{P}}(i,j)u_{i,j} + \mathcal{K}_{\mathrm{N}}(i,j)u_{i,j+1} + \mathcal{K}_{\mathrm{S}}(i,j)u_{i,j-1} = \mathrm{RHS}(i,j), \tag{12}$$

its matrix coefficients do observe the criterion :

$$\mathcal{K}_{\mathrm{E}}(i,j) = \mathcal{K}_{\mathrm{W}}(i+1,j), \tag{13a}$$
$$\mathcal{K}_{\mathrm{N}}(i,j) = \mathcal{K}_{\mathrm{S}}(i,j+1). \tag{13b}$$

We will consider here the discretization of the flux $F^{\mathrm{d}}_{\mathrm{n}}$ given by Eq. (4), that reads after midpoint discretization :

$$F^{\mathrm{d}}_{\mathrm{n}} \cong \widetilde{\Delta x}_i \, \frac{\partial u}{\partial y}(x_i, y_n), \tag{14}$$

where $y_n = y_j$ if $\Omega^u_{i,j+1}$ is a fluid cell (*i.e.* , $\theta^u_{i,j+1} > 0$), or otherwise $y_n = y^{\mathrm{c}}_j + \frac{1}{2}\,\theta^u_{i,j}\,\Delta y_j$ as in Fig. 2. Then, the differentiation of the linear interpolant of $u(x_i, y)$ in $[y^{\mathrm{c}}_j, y_n]$ gives :

$$\frac{\partial u}{\partial y}(x_i, y_n) \cong \begin{cases} \dfrac{u_{i,j+1} - u_{i,j}}{\frac{1}{2}\,\theta^u_{i,j}\,\Delta y_j + \frac{1}{2}\,\theta^u_{i,j+1}\,\Delta y_{j+1}} & \text{if } \theta^u_{i,j+1} > 0, \\ \dfrac{u(x_i, y_n) - u_{i,j}}{\frac{1}{2}\,\theta^u_{i,j}\,\Delta y_j} & \text{if } \theta^u_{i,j+1} = 0, \end{cases} \tag{15}$$

with $u(x_i, y_n) = 0$ in the last case since no-slip condition are imposed at the irregular boundary. Discretization (14),(15) generalizes the Cartesian case, and leads to a symmetric matrix verifying criterion (13).

Discretization of the convective fluxes

Similar considerations on the symmetries of the Navier-Stokes system shall guide the discretization of the convective flux (3a) across Γ^u. We aim now for a central discretization of the form $\mathcal{C}[\overline{U}]U$, where $\mathcal{C}[\overline{U}]$ is a skew-symmetric matrix, which verifies thus :

$$\begin{aligned}
\mathcal{C}[\overline{U}]_{\mathrm{P}}(i,j) &= 0 && (16a)\\
\mathcal{C}[\overline{U}]_{\mathrm{E}}(i,j) &= -\mathcal{C}[\overline{U}]_{\mathrm{W}}(i+1,j), && (16b)\\
\mathcal{C}[\overline{U}]_{\mathrm{N}}(i,j) &= -\mathcal{C}[\overline{U}]_{\mathrm{S}}(i,j+1). && (16c)
\end{aligned}$$

Consider now the flux $F_{\mathrm{n}}^{\mathrm{c}}$ across the face Γ_{n}^{u}, which is first discretized as the product of the mean value of u and the mass flux $\overline{v}_{\mathrm{n}}$ across this face :

$$F_{\mathrm{n}}^{\mathrm{c}} \cong u(x_i, y_n)\overline{v}_{\mathrm{n}}. \tag{17}$$

Then, the mass flux should be consistently discretized with the discrete continuity equation (10), as :

$$\overline{v}_{\mathrm{n}} \cong \tfrac{1}{2}\,\theta_{i,j}^{v}\,\overline{v}_{i,j} + \tfrac{1}{2}\,\theta_{i+1,j}^{v}\,\overline{v}_{i+1,j}, \tag{18}$$

and constant weight interpolation should be used to interpolate $u(x_i, y_n)$, *i.e.* :

$$u(x_i, y_n) \cong \begin{cases} \tfrac{1}{2}u_{i,j} + \tfrac{1}{2}u_{i,j+1} & \text{if } \theta_{i,j+1}^{u} > 0, \\ \tfrac{1}{2}u_{i,j} + 0 & \text{if } \theta_{i,j+1}^{u} = 0. \end{cases} \tag{19}$$

After performing similar discretization at all other faces, one gets a skew-symmetric matrix with coefficients that read :

$$\mathcal{C}[\overline{U}]_{\mathrm{P}}(i,j) \equiv \frac{1}{4}\,\mathrm{Cont}(\Omega_{i,j}) + \frac{1}{4}\,\mathrm{Cont}(\Omega_{i+1,j}) = 0, \tag{20a}$$

since the discrete continuity (10) is satisfied in each fluid cell, and :

$$\begin{aligned}
\mathcal{C}[\overline{U}]_{\mathrm{E}}(i,j) &\equiv \tfrac{1}{4}\,\theta_{i,j}^{u}\,\overline{u}_{i,j} + \tfrac{1}{4}\,\theta_{i+1,j}^{u}\,\overline{u}_{i+1,j}, && (20b)\\
\mathcal{C}[\overline{U}]_{\mathrm{N}}(i,j) &\equiv \tfrac{1}{4}\,\theta_{i,j}^{v}\,\overline{v}_{i,j} + \tfrac{1}{4}\,\theta_{i+1,j}^{v}\,\overline{v}_{i+1,j}. && (20c)
\end{aligned}$$

while the south and west coefficients are deduced from criterion (16).

Further computational details

In our method, we consider that the pressure unknown is merely a lagrangian multiplier that enforces the discrete continuity constraint (10) in all fluid cells. Thus, the discrete pressure $p_{i,j}$, located at $\boldsymbol{x}_{i,j}^{c}$, should be computed if $\Omega_{i,j}$ is a fluid cell (*i.e.* if the cell face ratio is non zero for at least two faces). The pressure gradient in the momentum equation (2) is simply discretized as :

$$\int_{\Gamma^u} p\,\boldsymbol{e}_x \cdot \boldsymbol{n} \;\, \mathrm{d}S \cong \Delta y_j \,(p_{i+1,j} - p_{i,j}). \tag{21}$$

The volume integrals in cell cuts are not computed using informations from the level set, since it would destroy the simple Cartesian structure of the linear systems, and thus severely diminishing the computational efficiency of the method. Instead, the time derivative term in the momentum equation is simply computed as :

$$\frac{\mathrm{d}}{\mathrm{d}t}\int_{\Omega^u} u \;\, \mathrm{d}V \cong \widetilde{\Delta x}_i \Delta y_j \frac{\mathrm{d}u_{i,j}}{\mathrm{d}t}. \tag{22}$$

The time stepping method we use is the semi-implicit AB/BDF2 projection scheme (see *e.g.* Botella et al.[2]). With out LS-MAC discretization, the pressure Poisson equation of the projection step is a symmetric linear system, as in the Cartesian case.This linear system is efficiently solved with the black-box multigrid solver of van Kan et al.[16].

3 Numerical results

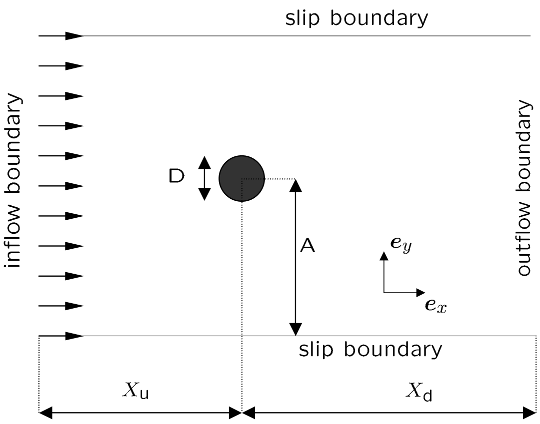

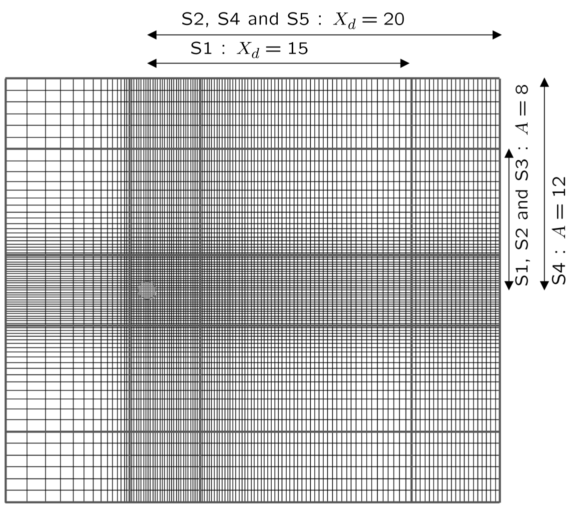

Figure 3: At left : geometry and boundary conditions of the flow over a circular cylinder. At right : mesh from simulation S4. One mesh line out of three is shown in both direction.

We have validated our method on the unsteady flow around a circular cylinder in a free-stream. The Reynolds number is defined as $Re = U_\infty D/\nu$, where U_∞ is the constant inlet velocity, D the cylinder diameter, and ν the kinematic viscosity. The lengths, velocities and times given in the following are scaled with D, U_∞ and D/U_∞ respectively.

The flow configuration is sketched in Fig. 3 (left). The initial condition is fluid at rest. At the inlet boundary, which is located at $X_u = 8$ units upstream of the obstacle, a uniform velocity profile is prescribed. At the outlet, which is located at X_d units downstream the cylinder, we use an improvement of the convective outflow condition based on the ghost-cell concept, which allows the use of the local convective velocity at the outlet instead of an *ad hoc* bulk velocity[3]. Slip conditions are prescribed at the horizontal boundaries. The distance A between these boundaries and the center of the cylinder is commonly referred to as the solid blockage of the flow. The values of X_d and A will be given later.

We use non-uniform Cartesian meshes refined in the wake of the cylinder as shown in Fig. 3 (right), with $N_x \times N_y$ cells. In the vicinity of the cylinder, the cell distribution is uniform of size h. For a shape as simple as a cylinder profile with unit diameter, the level set function takes the simple analytic expression :

$$\phi(x,y) = \frac{1}{2} - \sqrt{(x-x_{\mathrm{C}})^2 + (y-y_{\mathrm{C}})^2}\,,$$

where $(x_{\mathrm{C}},\, y_{\mathrm{C}})$ is the cylinder center. This expression is discretized at cell corners prior to the time integration.

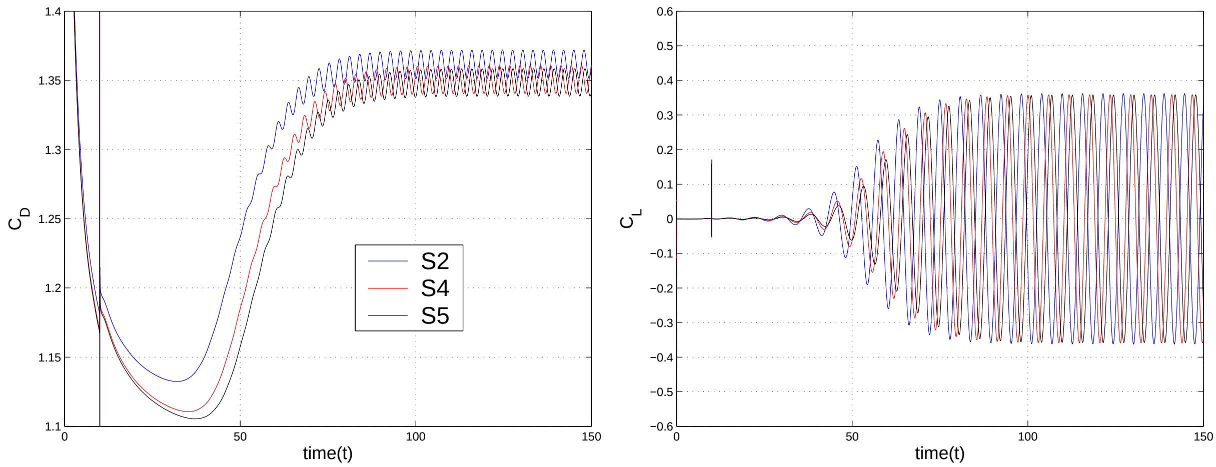

Figure 4: The drag (left) and lift (right) histories at Re = 100 for various values of the solid blockage A.

We have computed the time-periodic flow at Re = 100 and 200. In order to trigger the flow instability, we add an asymmetric disturbance $\boldsymbol{\delta v}(y)$ to the uniform inlet profile, defined by :

$$\boldsymbol{\delta v}(y) = \delta v_0 \tanh\left[\tfrac{1}{2}(y-y_{\mathrm{C}})\right]\boldsymbol{e}_x, \quad \delta v_0 = 10^{-2}.$$

This disturbance is removed at $t = 10$, giving rise to a singularity in the time evolution of the flow (see *e.g.* Figure 4). Once the flow reached an asymptotically periodic state at $t = 120$, we started computing the drag (C_{D}) and lift (C_{L}) coefficients at each time step until $t = 400$. The Strouhal number St is computed as the first harmonic of the power spectrum of the lift coefficient. The frequency resolution si $\pm 1.8 \times 10^{-3}$ since the length of the time signal is equal to 280 units.

	$N_x \times N_y$	A	X_d	Δt	h	St	$\overline{C}_\mathrm{D}$	$C_{\mathrm{L}_\mathrm{max}}$
S1	300×220	8	15	1.0×10^{-2}	0.040	0.172	1.361	0.361
S2	336×220	8	20	1.0×10^{-2}	0.040	0.172	1.362	0.359
S3	372×220	8	25	1.0×10^{-2}	0.040	0.172	1.362	0.362
S4	336×260	12	20	1.0×10^{-2}	0.040	0.172	1.351	0.359
S5	336×300	16	20	1.0×10^{-2}	0.040	0.172	1.349	0.358
S6	473×367	12	20	1.0×10^{-2}	0.028	0.172	1.346	0.358
S7	473×367	12	20	5.0×10^{-3}	0.028	0.172	1.346	0.358

Table 1: Summary of the cylinder flow computations at Re = 100. $\overline{C}_\mathrm{D}$: time average of drag coefficient. $C_{\mathrm{L}_\mathrm{max}}$: peak value of lift coefficient.

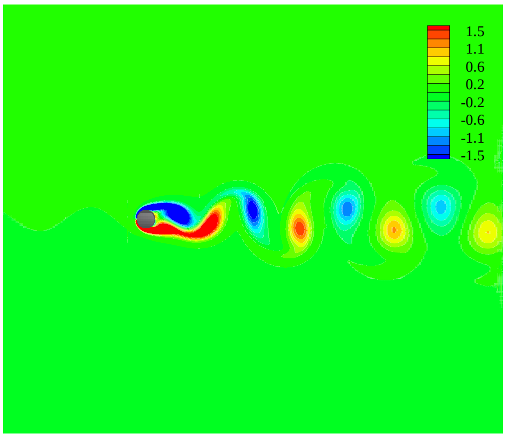

Figure 5: Vorticity field at $t = 400$ for the flow at Re = 100.

For the flow at Re = 100, we have studied the influence of various computational parameters such as the locations of the outflow boundary X_d and solid blockage A, grid resolution h and time step Δt. Table 1 sums up the different simulations, and an illustration of the vortex shedding at Re = 100 is given in Figure 5.

The first 5 simulations only concern the effect of boundaries positioning. For this purpose, the grids generated for simulations S2, S3, S4 and S5 are simply an expansion of the S1 grid with uniform mesh blocks, as shown in Figure 3 (right). First, we have studied the effects of the outlet boundary position on computations S1, S2 and S3. The discrepancy in the results displayed in Table 1 is very slight, showing that $X_\mathrm{d} = 20$ is long enough for the following simulations. Then, simulations S2, S4 and S5 are carried out to study the solid blockage effect. We observe that grid independence is obtained for $A \geq 12$, as shown in Figure 4 and Table 1. The last two simulations concerns the spacial and temporal accuracy. Simulation S6 and S7 have the same computational parameters as S4, except that S6 uses twice more points and S7 uses a halved time step. These

	St	$\overline{C}_D$	$C_{L_{max}}$
***Re* = 100**			
Wieselberger[18] (1921)	-	1.21-1.41	-
Berger and Wille[1] (1972)	0.16-0.17	-	-
Linnick and Fasel[10] (2005)	0.166	1.34±0.009	0.333
Persillon and Braza[14] (1998)	0.165	1.253	0.395
Majander and Siikonen[11] (2002)	0.171	1.356	0.319
Present work	0.172±0.0018	1.346	0.358
***Re* = 200**			
Wieselberger[18] (1921)	-	1.29	-
Berger and Wille[1] (1972)	0.18-0.19	-	-
Linnick and Fasel[10] (2005)	0.197	1.34±0.044	0.69
Persillon and Braza[14] (1998)	0.198	1.321	0.776
Majander and Siikonen[11] (2002)	0.191	1.319	0.647
Present work	0.201±0.0018	1.368	0.722

Table 2: Summary of results on the cylinder flow at Re = 100 and Re = 200.

simulations shows the independence of our results from the computational parameters.

Finally, Table 2 displays selected results from previous experimental[1,18] and numerical[10,11,14] studies, and compares them with the computations obtained on our most refined mesh (S7). Linnick and Fasel[10] use a fourth-order immersed boundary method on Cartesian grids, while Persillon and Braza[14] uses second-order finite-volume method on curvilinear grids. Majander and Siikonen[11] performed a comprehensive study on the accuracy of various time stepping schemes, and arguably gives the most reliable results. Our simulations show a good agreement with these results. However, we note that the value of the Strouhal number at Re = 100 is closer to the one obtained by Majander and Siikonen[11] than the other numerical studies.

References

[1] E. Berger and R. Wille. Periodic flow phenomena. *Ann. Rev. Fluid Mech.*, **4**, 313-340, 1972.

[2] O. Botella, M. Y. Forestier, R. Pasquetti, R. Peyret, and C. Sabbah. Chebyshev methods for the Navier-Stokes equations : Algorithms and applications. *Nonlinear Analysis*, **47**, 4157-4168, 2001.

[3] Y. Cheny and O. Botella. *In preparation.*

[4] M. Dröge and R. Verstappen. A new symmetry-preserving Cartesian-grid method for computing flow past arbitrarily shaped objects. *Int. J. Numer. Meth. Fluids*, **47**, 979-985, 2005.

[5] E. A. Fadlun, R. Verzicco, P. Orlandi, and J. Mohd-Ysof. Combined immersed-boundary finite-difference methods for three dimensional complex flow simulations. *J. Comput. Phys.*, **161**, 35-60, 2000.

[6] J. H. Ferziger and M. Periȅ. *Computational Methods for Fluid Dynamics.* Springer, Berlin, 1996.

[7] F. Gibou, R. P. Fedkiw, Li-Tien Cheng, and M. Kang. A second-order-accurate symmetric discretization of the Poisson equation on irregular domains. *J. Comput. Phys.*, **176**, 205-227, 2002.

[8] F. H. Harlow and J. E. Welch. Numerical calculation of time-dependent viscous incompressible flow of fluid with free surfaces. *Phys. Fluids*, **8**, 2181-2189, 1965.

[9] S. Kang, G. Iaccarino, and P. Moin. Accurate and efficient immersed-boundary interpolations for viscous flows. In *Center for Turbulence Research Briefs,* pp. 31-43, 2004.

[10] M. N. Linnick and H. F. Fasel. A high order immersed interface method for simulating unsteady incompressible flows on irregular domains. *J. Comput. Phys.*, **204**, 157-192, 2005.

[11] P. Majander and T. Siikonen. A comparison of time integration methods in a unsteady low-Reynolds-number flow. *Int. J. Numer. Meth. Fluids.*, **39**, 361-390, 2002.

[12] R. Mittal and G. Iaccarino. Immersed boundary methods. *Annu. Rev. Fluid Mech.*, **37**, 239-261, 2005.

[13] S. Osher and R. Fedkiw. *Level Set Methods and Dynamic Implicit Surfaces.* Springer, New-York, 2003.

[14] H. Persillon and M. Braza. Physical analysis of the transition to turbulence in the wake of a circular cylinder by three dimensional Navier-Stokes simulation. *J. Fluid Mech.*, **365**, 23-88, 1998.

[15] P. G. Tucker and Z. Pan. A cartesian cut cell method for incompressible viscous flow. *Appl Math. Modelling*, **24**, 591-606, 2000.

[16] J. van Kan, C. Vuik, and P. Wesseling. Fast pressure calculation for 2D and 3D time dependent incompressible flow. *Numer. Linear Algebra Appl.*, **7**, 429-447, 2000.

[17] R. W. C. P. Verstappen and A. E. P. Veldman. Symmetry-preserving discretization of turbulent flow. *J. Comput. Phys.*, **187**, 343-368, 2003.

[18] C. Wieselberger. New data on the law of hydro and aerodynamic resistance (in german). *Physikalische Zeitschrift*, **23**, 24-219, 1921.